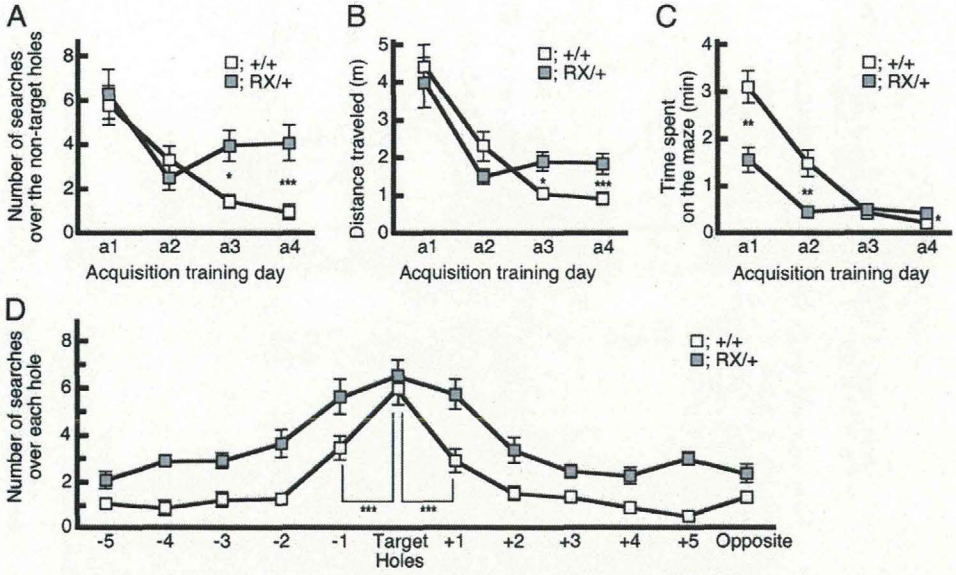

Fig. 5. *Scn1a*$^{RX/+}$ mice show lowered spatial learning ability in the Barnes maze test. (A–C) Results in acquisition training trials on days 1–4 (a1–a4). Eleven *Scn1a*$^{+/+}$ mice and 11 *Scn1a*$^{RX/+}$ mice were analyzed. (A) The numbers of searches over non-target holes on days a3 and a4 were higher in *Scn1a*$^{RX/+}$ mice than in *Scn1a*$^{+/+}$ mice (two-way ANOVA; main effect genotype: $F(1, 64) = 4.9$, $p<0.05$; main effect day: $F(3, 192) = 12.6$, $p<0.001$; interaction: $F(3, 192) = 3.7$, $p<0.05$; Mann–Whitney *U* test; day a3: $p<0.05$; day a4: $p<0.001$). In *Scn1a*$^{+/+}$ mice, the number of searches over non-target holes was progressively reduced over the course of acquisition training trials (paired *t*-test; day a1 vs. day a2: $p<0.05$; day a2 vs. day a3: $p<0.05$; day a3 vs. day a4: p = ns). In *Scn1a*$^{RX/+}$ mice, the number of searches over non-target holes was reduced from day a1 to day a2, but not improved after day a2 (paired *t*-test; day a1 vs. day a2: $p<0.01$; day a2 vs. day a3: p = ns; day a3 vs. day a4: p = ns). (B) Distances traveled on days a3 and a4 were greater in *Scn1a*$^{RX/+}$ mice than in *Scn1a*$^{+/+}$ mice (two-way ANOVA; main effect genotype: $F(1, 64) = 0.2$, p = ns; main effect day: $F(3, 192) = 27.0$, $p<0.001$; interaction: $F(3, 192) = 2.9$, $p<0.05$; Mann–Whitney *U* test; day a3: $p<0.05$; day a4: $p<0.001$). In *Scn1a*$^{+/+}$ mice, distance traveled was progressively reduced over the course of acquisition training trials (paired *t*-test; day a1 vs. day a2: $p<0.001$; day a2 vs. day a3: $p<0.01$; day a3 vs. day a4: p = ns). In *Scn1a*$^{RX/+}$ mice, distance traveled was reduced from day a1 to day a2, but not improved after day a2 (paired *t*-test; day a1 vs. day a2: $p<0.01$; day a2 vs. day a3: p = ns; day a3 vs. day a4: p = ns). (C) Time spent in the maze by *Scn1a*$^{RX/+}$ mice was shorter than that in *Scn1a*$^{+/+}$ mice on days a1 and a2, but longer on day a4 (two-way ANOVA; main effect genotype: $F(1, 64) = 12.7$, $p<0.01$; main effect day: $F(3, 192) = 56.1$, $p<0.001$; interaction: $F(3, 192) = 11.8$, $p<0.001$; Mann–Whitney *U* test; day a1: $p<0.01$; day a2: $p<0.01$; day a4: $p<0.05$). In *Scn1a*$^{+/+}$ mice, time spent in the maze was progressively reduced over the course of acquisition training trials (paired *t*-test; day a1 vs. day a2: $p<0.001$; day a2 vs. day a3: $p<0.001$; day a3 vs. day a4: $p<0.05$). In *Scn1a*$^{RX/+}$ mice, time spent in the maze was reduced from day a1 to day a2, but not improved after day a2 (paired *t*-test; day a1 vs. day a2: $p<0.001$; day a2 vs. day a3: p = ns; day a3 vs. day a4: p = ns). (D) Number of searches of each hole in the probe test after acquisition training. *Scn1a*$^{RX/+}$ mice showed a lesser preference for the target hole than *Scn1a*$^{+/+}$ mice (*Scn1a*$^{+/+}$ mice: one-way ANOVA; hole: $F(11, 110) = 24.4$, $p<0.001$; paired *t*-test; −1 hole vs. target: $p<0.001$; target vs. +1 hole: $p<0.001$; *Scn1a*$^{RX/+}$ mice: one-way ANOVA; hole: $F(11, 110) = 13.0$, $p<0.001$; paired *t*-test; −1 hole vs. target: p = ns; target vs. +1 hole: p = ns). Eleven *Scn1a*$^{+/+}$ mice and 11 *Scn1a*$^{RX/+}$ mice were analyzed. Data represent means ± SEM, $^{*}p<0.05$, $^{**}p<0.01$, $^{***}p<0.001$.

training trials. These observations suggested that the lowered reversal task learning ability of *Scn1a*$^{RX/+}$ mice was not due to rigidity and insistence on sameness but largely due to lowered spatial learning ability.

We next performed the probe test after reversal training (Fig. 6E). While *Scn1a*$^{+/+}$ mice predominantly preferred the target hole to adjacent non-target holes, *Scn1a*$^{RX/+}$ mice showed a weaker preference than *Scn1a*$^{+/+}$ mice. These results provided additional evidence suggesting that *Scn1a*$^{RX/+}$ mice had a lowered learning ability.

Overall, the Barnes maze test showed that *Scn1a*$^{RX/+}$ mice have a lowered spatial learning ability, which might be of relevance to the visuo-perceptual impairment in Dravet syndrome patients (Cassé-Perrot et al., 2001; Chieffo et al., 2011; Dravet et al., 2005; Wolff et al., 2006).

Scn1a$^{RX/+}$ mice have a normal gait appearance

A mild motor discoordination has been reported in heterozygous *Scn1a* knockout mice (Kalume et al., 2007). We assessed motor coordination and balance in *Scn1a*$^{RX/+}$ male mice using an accelerating rotarod test. The latency to fall off the rotarod was longer in *Scn1a*$^{RX/+}$ mice than in *Scn1a*$^{RX/+}$ mice at days 1 and 2 (Fig. 7A). The latency in *Scn1a*$^{+/+}$ mice was significantly increased at day 3, and reached a similar level to that in *Scn1a*$^{RX/+}$ mice at days 3 and 4. The body weight of the *Scn1a*$^{RX/+}$ mice subjected to the rotarod test was similar to that of *Scn1a*$^{+/+}$ controls (8-week-old: 24.35 ± 0.79 g for *Scn1a*$^{+/+}$ mice; 25.52 ± 0.59 g for *Scn1a*$^{RX/+}$ mice; Mann–Whitney *U* test; p = ns), and therefore seemed not to contribute to better performance of *Scn1a*$^{RX/+}$ mice in the first two trials.

We subsequently assessed motor behaviors of *Scn1a*$^{RX/+}$ male mice using a footprint test. As shown in Figs. 7B–E, there were no significant differences in stride length, hindbase width, frontbase width, and front/hind footprint overlap between the genotypes. The normal gait appearance of *Scn1a*$^{RX/+}$ mice is inconsistent with motor discoordination of heterozygous *Scn1a* knockout mice (Kalume et al., 2007).

Adult *Scn1a*$^{RX/+}$ mice have normal background/interictal EEG activity

It was recently suggested that the mental outcomes of Dravet syndrome adolescents could be linked to a lack of occipital alpha rhythms in their background/interictal EEG activity (Akiyama et al., 2010). To examine whether there was any abnormal background/interictal EEG activity in adult *Scn1a*$^{RX/+}$ mice, we performed EEG recordings in adult *Scn1a*$^{+/+}$ and *Scn1a*$^{RX/+}$ mice (Fig. 8). Some *Scn1a*$^{RX/+}$ mice show recurrent spontaneous seizures after P18 (Ogiwara et al., 2007), but the employed mice in the present study showed no seizures at least during the EEG recordings. Background/interictal EEG activities in the cortex and hippocampus in each of the three stages, including slow-wave sleep, REM sleep and waking stages, did not differ between genotypes. The relative ratio of EEG power at respective frequency bands also showed no differences between genotypes in any of the stages (data not shown). Thus, we failed

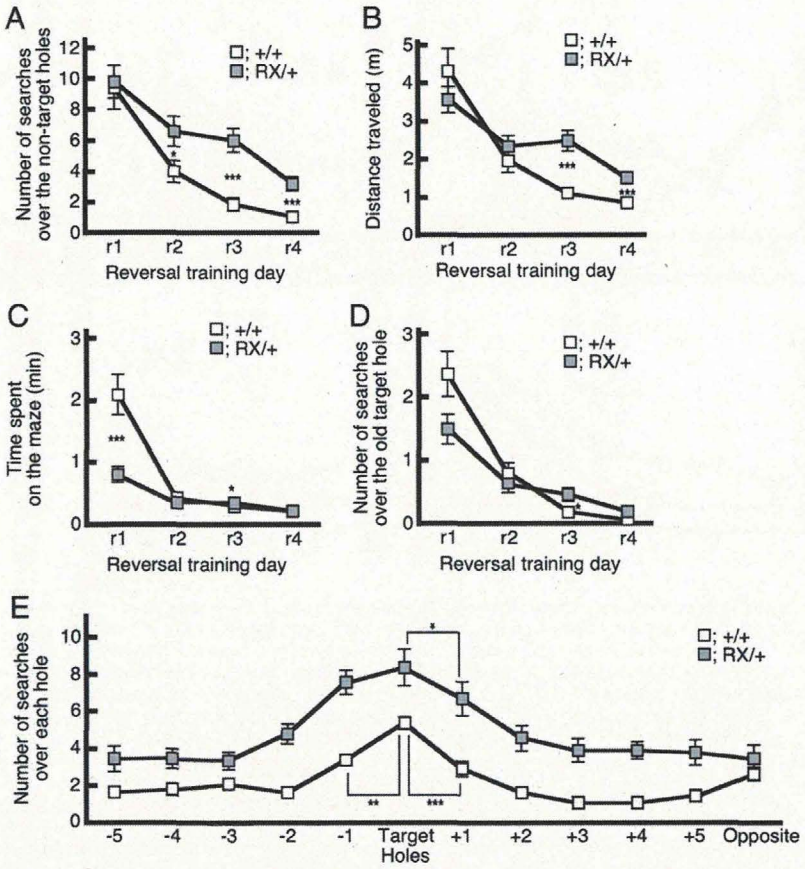

Fig. 6. *Scn1a*$^{RX/+}$ mice show lowered reversal learning ability in the Barnes maze test. (A–D) Results of reversal training trials on days 8–11 (r1–r4), days counted from the acquisition training. Eleven *Scn1a*$^{+/+}$ mice and 11 *Scn1a*$^{RX/+}$ mice were analyzed. (A) The numbers of searches over non-target holes on days r2, r3 and r4 were higher in *Scn1a*$^{RX/+}$ mice than in *Scn1a*$^{+/+}$ mice (two-way ANOVA; main effect genotype: $F(1, 64) = 1.1$, p = ns.; main effect day: $F(3, 192) = 45.0$, $p<0.001$; interaction: $F(3, 192) = 2.5$, $p<0.01$; Mann–Whitney *U* test; day r2: $p<0.05$; day r3: $p<0.001$; day r4: $p<0.001$). In *Scn1a*$^{+/+}$ mice, the number of searches over non-target holes was progressively reduced over the course of reversal training trials (paired *t*-test; day r1 vs. day r2: $p<0.001$; day r2 vs. day r3: $p<0.01$; day r3 vs. day r4: p = ns). In *Scn1a*$^{RX/+}$ mice, while the number of searches over non-target holes was reduced from day r1 to day r2 and from day r3 to day r4, it was not reduced from day r2 to day r3 (paired *t*-test; day r1 vs. day r2: $p<0.05$; day r2 vs. day r3: p = ns; day r3 vs. day r4: $p<0.01$). (B) The distance traveled on days r3 and r4 was greater in *Scn1a*$^{RX/+}$ mice than in *Scn1a*$^{+/+}$ mice (two-way ANOVA; main effect genotype: $F(1, 64) = 2.5$, p = ns; main effect day: $F(3, 192) = 32.6$, $p<0.001$; interaction: $F(3, 192) = 4.7$, $p<0.01$; Mann–Whitney *U* test; day r3: $p<0.001$; day r4: $p<0.001$). In *Scn1a*$^{+/+}$ mice, distance traveled was progressively reduced over the course of reversal training trials (paired *t*-test; day r1 vs. day r2: $p<0.01$; day r2 vs. day r3: $p<0.01$; day r3 vs. day r4: p = ns). In *Scn1a*$^{RX/+}$ mice, while distance traveled was reduced from day r1 to day r2 and from day r3 to day r4, it was not reduced from day r2 to day r3 (paired *t*-test; day r1 vs. day r2: $p<0.01$; day r2 vs. day r3: p = ns; day r3 vs. day r4: $p<0.01$). (C) Time spent in the maze by *Scn1a*$^{RX/+}$ mice was shorter than that spent by *Scn1a*$^{+/+}$ mice on day r1 but longer on day r3 (two-way ANOVA; main effect genotype: $F(1, 64) = 10.2$, $p<0.01$; main effect day: $F(3, 192) = 41.1$, $p<0.001$; interaction: $F(3, 192) = 12.7$, $p<0.001$; Mann–Whitney *U* test; day r1: $p<0.05$; day r3; Mann–Whitney *U* test; $p<0.05$). In *Scn1a*$^{+/+}$ mice, time spent in the maze was progressively reduced over the course of reversal training trials (paired *t*-test; day r1 vs. day r2: $p<0.001$; day r2 vs. day r3: p = ns; day r3 vs. day r4: p = ns). In *Scn1a*$^{RX/+}$ mice, while time spent in the maze was reduced from day r1 to day r2 and from day r3 to day r4, it was not improved from day r2 to day r3 (paired *t*-test; day r1 vs. day r2: $p<0.001$; day r2 vs. day r3: p = ns; day r3 vs. day r4: $p<0.01$). (D) The number of searches over the old target hole was progressively reduced in both *Scn1a*$^{+/+}$ and *Scn1a*$^{RX/+}$ mice over the course of reversal training trials (*Scn1a*$^{+/+}$ mice: paired *t*-test; day r1 vs. day r2: $p<0.001$; day r2 vs. day r3: $p<0.01$; day r3 vs. day r4: p = ns; *Scn1a*$^{RX/+}$ mice: paired *t*-test; day r1 vs. day r2: $p<0.01$; day r2 vs. day r3: p = ns; day r3 vs. day r4: $p<0.05$). The number of searches over the old target hole on days r1, r2 and r4 was similar in *Scn1a*$^{+/+}$ and *Scn1a*$^{RX/+}$ mice (two-way ANOVA; main effect genotype: $F(1, 64) = 4.9$, $p<0.05$; main effect day: $F(3, 192) = 12.6$, $p<0.001$; interaction: $F(3, 192) = 3.7$, $p<0.05$; Mann–Whitney *U* test; days r1, r2 and r4: p = ns; day r3: $p<0.05$). (E) Number of searches of each hole in the probe test after reversal training. *Scn1a*$^{RX/+}$ mice showed a lesser preference for the target hole than *Scn1a*$^{+/+}$ mice (*Scn1a*$^{+/+}$ mice: one-way ANOVA; hole: $F(11, 110) = 14.3$, $p<0.001$; paired *t*-test; −1 hole vs. target: $p<0.01$; target vs. +1 hole: $p<0.001$; *Scn1a*$^{RX/+}$ mice: one-way ANOVA; hole: $F(11, 88) = 7.2$, $p<0.001$; paired *t*-test; −1 hole vs. target: p = ns; target vs. +1 hole: $p<0.05$). Eleven *Scn1a*$^{+/+}$ and 9 *Scn1a*$^{RX/+}$ mice were analyzed. Data represent means ± SEM, $^{*}p<0.05$, $^{**}p<0.01$, $^{***}p<0.001$.

to find any abnormalities in background EEG activity in *Scn1a*$^{RX/+}$ mice in the adult stage.

Discussion

In this study, we found that *Scn1a*$^{RX/+}$ mice have novelty-induced hyperactivity, low sociability and poor spatial learning ability. Thereby, the *Scn1a*$^{RX/+}$ mice constitute a useful tool for understanding the pathologic process of cognitive decline and behavioral abnormalities in Dravet syndrome patients in addition to their epileptic seizure phenotypes.

Cognition and behaviors of Dravet syndrome patients often show a characteristic evolutional feature as the patients grow up (Cassé-Perrot et al., 2001; Dravet et al., 2005). Before the age of one year and after onset, cognition and behaviors seem to be normal while prolonged convulsive seizures are marked. During the second year of life, cognitive decline and behavioral abnormalities including autistic ones become apparent while additional multiple seizure types including myoclonic seizures, atypical absence seizures and complex partial seizures emerge and occur with high frequency. The coincidence of cognitive and behavioral abnormalities and a high frequency of multiple types of seizures during the second and third years of life might suggest that epileptic seizures affect a child's cognitive and behavioral growth. However,

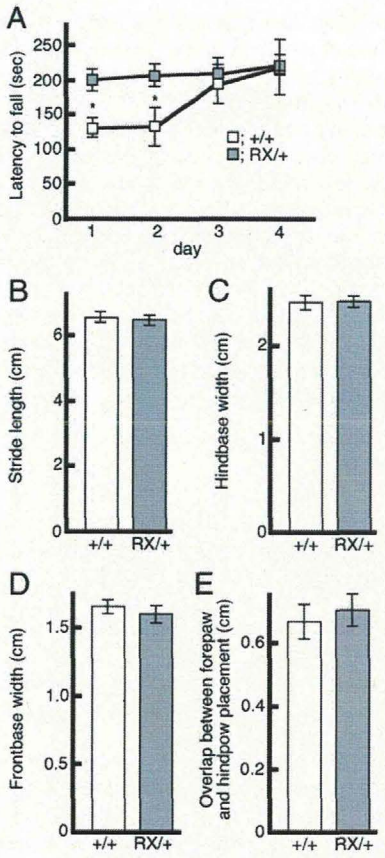

Fig. 7. *Scn1a*$^{RX/+}$ mice have a normal gait. (A) The results of the accelerating rotarod test. *Scn1a*$^{RX/+}$ mice performed better than *Scn1a*$^{+/+}$ mice at days 1 and 2 (two-way ANOVA; main effect genotype: $F(1, 14) = 3.0$, p = ns; main effect day: $F(3, 12) = 4.2$, $p < 0.05$; interaction: $F(3, 12) = 2.3$, p = ns; Mann–Whitney *U* test; day 1: $p < 0.05$; day 2: $p < 0.05$; day 3: p = ns; day 24: p = ns). *Scn1a*$^{+/+}$ mice showed a progressive increase in the latency over the course of training trials (paired *t*-test; day 1 vs. day 2: p = ns; day 2 vs. day 3: $p < 0.05$; day 3 vs. day 4: p = ns). *Scn1a*$^{RX/+}$ mice also had a slight, but not statistically significant increase in the latency over the course of training trials (paired *t*-test; day 1 vs. day 2: p = ns; day 2 vs. day 3: p = ns; day 3 vs. day 4: p = ns). (B–E) Results of the footprint test. Stride length (B), hindbase width (C), frontbase width (D), and front/hind footprint overlap (E) were similar in *Scn1a*$^{+/+}$ mice and *Scn1a*$^{RX/+}$ mice (Mann–Whitney *U* test; p = ns). The white and grey bars represent *Scn1a*$^{+/+}$ and *Scn1a*$^{RX/+}$ mice, respectively ($n = 8$, each group). Data represent means ± SEM, $^{*}p < 0.05$.

there is a weak correlation between cognitive function levels and seizure phenotypes (Riva et al., 2009). In addition, while cognitive functions are impaired in all patients, patients develop different seizure types with varying frequencies and a high frequency of seizures and early appearance of myoclonic and absence seizures are not always associated with severe cognitive decline (Ragona et al., 2010; Wolff et al., 2006). These observations suggest that the epileptic seizures are not only the causal factor for autistic-like behavior and cognitive decline of Dravet syndrome patients.

In the present study, *Scn1a*$^{RX/+}$ mice showed impaired spatial learning, which is generally thought to require hippocampus function (Barnes, 1979). We previously reported that $Na_v1.1$ is predominantly expressed at axons and somata of parvalbumin-positive (PV) inhibitory interneurons in mouse neocortex and hippocampus, and that the neocortical fast-spiking interneurons, which should be regarded as PV interneurons (Kawaguchi and Kondo, 2002), of *Scn1a*$^{RX/+}$ mice exhibited a pronounced spike amplitude decrement late in the burst (Ogiwara et al., 2007). Reduced sodium currents in GABAergic inhibitory neurons in another $Na_v1.1$-deficient mouse have also been reported in the hippocampus (Yu et al., 2006). Other studies showed that selective impairment or ablation of PV + interneurons in hippocampus induced spatial working memory impairments (Korotkova et al., 2010; Murray et al., 2011). These observations suggest that, although epileptic seizures may partially contribute to and aggravate the cognitive impairments of *Scn1a*$^{RX/+}$ mice, $Na_v1.1$ haploinsufficiency should directly impair the fundamental function of the hippocampal circuit and thereby cause spatial learning deficits in *Scn1a*$^{RX/+}$ mice and cognitive decline in Dravet syndrome patients. Dravet syndrome children show poor social interaction skills, which become apparent during early childhood and rarely rise above the level of those of a 2-year-old (Cassé-Perrot et al., 2001; Riva et al., 2009; Wolff et al., 2006). In the present study of the social interaction test, *Scn1a*$^{RX/+}$ mice neither made active approaches toward unfamiliar mice nor rejected contacts from unfamiliar actively-approaching mice, which well represented the autistic features of Dravet syndrome children. $Na_v1.1$ is widely expressed in brain including neocortex (Ogiwara et al., 2007), and therefore the haploinsufficiency of $Na_v1.1$ in *Scn1a*$^{RX/+}$ mice may impair the functions of the brain regions including those responsible for sociability such as prefrontal cortex, and as a fundamental cause it may have impaired social behavior of the mice.

Attention deficit and hyperactivity often occur in Dravet syndrome children (Caraballo and Fejerman, 2006; Cassé-Perrot et al., 2001; Dravet et al., 2005; Nolan et al., 2006; Ragona et al., 2010;

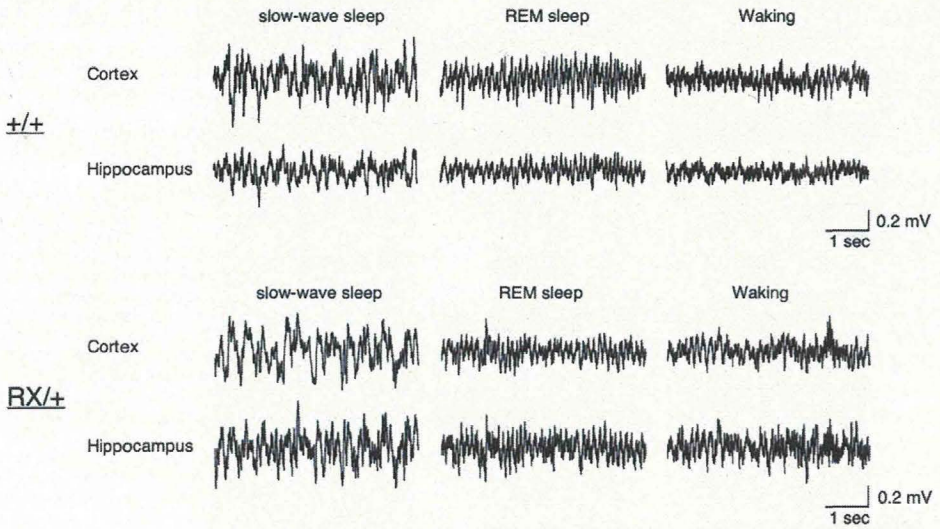

Fig. 8. Adult *Scn1a*$^{RX/+}$ mice show normal background/interictal EEG activity. EEG activity of cortex and hippocampus in slow-wave sleep, REM sleep and waking stages in adult *Scn1a*$^{+/+}$ (upper panel) and *Scn1a*$^{RX/+}$ (lower panel) mice ($n = 4$, each group). Representative results are shown.

Wolff et al., 2006). In the present study, we also observed hyperactivity in *Scn1a*$^{RX/+}$ mice exposed to novel environments although *Scn1a*$^{RX/+}$ mice are hypoactive in their home cages. This novelty-induced hyperactivity in *Scn1a*$^{RX/+}$ mice may be relevant to the hyperactive phenotype observed in Dravet syndrome patients. Hyperactivity would also be a modifying factor underlying the poor social interaction skills of Dravet syndrome children, because hyperactivity seems to prevent prolonged interpersonal contacts (Cassé-Perrot et al., 2001). Similarly, the novelty-induced hyperactivity may partially contribute to the altered social behaviors in *Scn1a*$^{RX/+}$ mice as well.

Ataxia usually appears in Dravet syndrome children from the second year of life (Dravet et al., 2005). Their imbalance gait tends to disappear after the fourth year of life, whereas some patients continue to have severe ataxia. We and others have reported severe ataxia in homozygous *Scn1a* knockout mice and knock-in (*Scn1a*$^{RX/RX}$) mice (Kalume et al., 2007; Ogiwara et al., 2007; Yu et al., 2006). Kalume and his colleagues have further found a mild motor discoordination in heterozygous *Scn1a* knockout mice (Kalume et al., 2007). Using the footprint test, they have shown that 3-week-old heterozygous *Scn1a* knockout mice have normal stride length but widened front/hind footprint overlap. In contrast, our present study of the footprint test indicated that 9-week-old *Scn1a*$^{RX/+}$ mice have a normal gait appearance. This inconsistency may be due to age differences of the mice. The normal gait appearance of *Scn1a*$^{RX/+}$ mice is consistent with their enhanced motor coordination observed in the first two trials in the accelerating rotarod test. The enhanced motor coordination may be related to the novelty-induced hyperactivity.

Dravet syndrome children show variable and unstable anxiety phenotypes, increased or decreased depends on occasions and individuals. In our present study of the open field test, *Scn1a*$^{RX/+}$ mice continued to spend less time in the center of the field (increased thigmotaxis) that suggested increased anxiety. On the other hand, in the elevated-plus maze test the mice spent more time in the open arm that suggested reduced anxiety. One possible explanation for this inconsistency is that the increased thigmotaxis does not indicate increased anxiety but caused by other reason(s) such as changed preference but the increased time in the open arm surely indicates reduced anxiety. Actually, such an increase of time spent in the open arm of elevated-plus maze have also been described in several rodent models of attention deficit and hyper-activity that were elucidated as reduced anxiety (Sontag et al., 2010; Trantham-Davidson et al., 2008). Conversely, the increased thigmotaxis may still indicate increased anxiety but the increased time in the open arm does not indicate reduced anxiety. Kalynchuk et al. (1997) previously reported increases of time spent in the open arm of elevated-plus maze observed in long-term amygdala kindling rats and elucidated it as increased anxiety or escaping behavior in novel environments. At present we do not have a confident explanation, and further studies are required to determine whether anxiety is increased or decreased in the *Scn1a*$^{RX/+}$ mice.

Abnormalities in neocortical and hippocampal PV interneurons have been described in various mouse models for neuropsychiatric disorders including ASDs. Reduced number of PV interneurons and density of PV-immunopositive fibers were described in hippocampus of mouse models for ASDs, such as *Cadps2* knockout mice and *Nrp2* knockout mice (Gant et al., 2009; Sadakata et al., 2007). Furthermore, a mouse model for Rett syndrome, which has autistic behaviors, an increased incidence of seizures and other neurological problems, showed abnormal development of neocortical PV interneurons (Fukuda et al., 2005). Similarly, in mouse models for fragile X syndrome, which has cognitive impairment, anxiety, autistic behaviors and an increased incidence of seizures, PV interneurons were reduced in number and showed enlarged somata and altered lamina distribution (Selby et al., 2007). It is thus plausible that altered function of PV inhibitory circuits, arising from $Na_v1.1$ haploinsufficiency, impacts on cognitive function and social behaviors in Dravet syndrome patients. Genetic manipulation of *Scn1a* gene in PV interneurons in mice (e.g., using a PV cell-specific Cre driver and a mouse line with a floxed *Scn1a* allele) should offer the opportunity to directly test whether PV interneuron dysfunction contributes to the pathophysiology of autistic-like behaviors and cognitive impairment.

In conclusion, our findings showed that, in addition to recurrent seizures (Ogiwara et al., 2007), $Na_v1.1$ haploinsufficiency in mice is enough to cause low sociability and spatial learning impairment in *Scn1a*$^{RX/+}$ mice. Although it has been proposed that polytherapy and long-term use of anticonvulsants have potentials to affect the cognitive function and behaviors of Dravet syndrome patients (Cassé-Perrot et al., 2001; Dravet et al., 2005), our present results on mouse models suggest that the $Na_v1.1$ haploinsufficiency is fundamentally responsible for the behavioral and cognitive impairments in Dravet syndrome patients and those impairments should occur in patients even without medications.

Acknowledgments

The authors would especially like to thank Dr. Shigeyoshi Itohara and Mr. Hiromichi Goto (Laboratory for Behavioral Genetics, RIKEN Brain Science Institute) for their generous gift of CAG-Flpe mice and help with the HomeCageScan, and Dr. Hirokazu Oguni (Department of Pediatrics, Tokyo Women's Medical University) for critical reading of the manuscript and valuable suggestions. We also thank Messrs. Atsushi Shimohata and Kenji Amano and Mses. Ikuyo Inoue, Emi Mazaki and Natsuko Tokonami (Laboratory for Neurogenetics, RIKEN Brain Science Institute) for technical support.

This work was supported in part by grants from the RIKEN Brain Science Institute; the Strategic Research Program for Brain Sciences and Grants-in-aid for Scientific Research of the Ministry of Education, Culture, Sports, Science and Technology of Japan; and the Kato Memorial Bioscience Foundation.

References

Akiyama, M., Kobayashi, K., Yoshinaga, H., Ohtsuka, Y., 2010. A long-term follow-up study of Dravet syndrome up to adulthood. Epilepsia 51, 1043–1052.
Barnes, C.A., 1979. Memory deficits associated with senescence: a neurophysiological and behavioral study in the rat. J. Comp. Physiol. Psychol. 93, 74–104.
Cao, D., Ohtani, H., Ogiwara, I., Ohtani, S., Takahashi, Y., Yamakawa, K., et al., 2012. Efficacy of stiripentol in hyperthermia-induced seizures in a mouse model of Dravet syndrome. Epilepsia 53, 1140–1145.
Caraballo, R.H., Fejerman, N., 2006. Dravet syndrome: a study of 53 patients. Epilepsy Res. 70 (Suppl. 1), S231–S238.
Carter, R.J., Morton, A.J., Dunnett, S.B., 2001. Motor coordination and balance in rodents. In: Taylor, G.P. (Ed.), Current Protocols in Neuroscience. John Wiley & Sons, Inc., New York, pp. 8.12.1–8.12.14.
Cassé-Perrot, C., Wolf, M., Dravet, C., 2001. Neuropsychological aspects of severe myoclonic epilepsy in infancy. In: Jambaqué, I., Lassonde, M., Dulac, O. (Eds.), Neuropsychology of Childhood Epilepsy. Kluwer Academic/Plenum Publishers, New York, pp. 131–140.
Chieffo, D., Ricci, D., Baranello, G., Martinelli, D., Veredice, C., Lettori, D., et al., 2011. Early development in Dravet syndrome: visual function impairment precedes cognitive decline. Epilepsy Res. 93, 73–79.
Claes, L., Del-Favero, J., Ceulemans, B., Lagae, L., Van Broeckhoven, C., De Jonghe, P., 2001. De novo mutations in the sodium-channel gene SCN1A cause severe myoclonic epilepsy of infancy. Am. J. Hum. Genet. 68, 1327–1332.
Depienne, C., Trouillard, O., Saint-Martin, C., Gourfinkel-An, I., Bouteiller, D., Carpentier, W., et al., 2009. Spectrum of SCN1A gene mutations associated with Dravet syndrome: analysis of 333 patients. J. Med. Genet. 46, 183–191.
Dravet, C., Bureau, M., Oguni, H., Fukuyama, Y., Cokar, O., 2005. Severe myoclonic epilepsy in infancy (Dravet syndrome). In: Roger, J., Bureau, M., Dravet, C., Genton, P., Tassinari, C.A., Wolf, P. (Eds.), Epileptic Syndromes in Infancy, Childhood and Adolescence, 4th ed. John Libbey Eurotext, Montrouge, pp. 89–113.
Escayg, A., MacDonald, B.T., Meisler, M.H., Baulac, S., Huberfeld, G., An-Gourfinkel, I., et al., 2000. Mutations of SCN1A, encoding a neuronal sodium channel, in two families with GEFS+2. Nat. Genet. 24, 343–345.
Fujiwara, T., Sugawara, T., Mazaki-Miyazaki, E., Takahashi, Y., Fukushima, K., Watanabe, M., et al., 2003. Mutations of sodium channel alpha subunit type 1 (SCN1A) in intractable childhood epilepsies with frequent generalized tonic–clonic seizures. Brain 126, 531–546.
Fukuda, T., Itoh, M., Ichikawa, T., Washiyama, K., Goto, Y., 2005. Delayed maturation of neuronal architecture and synaptogenesis in cerebral cortex of Mecp2-deficient mice. J. Neuropathol. Exp. Neurol. 64, 537–544.

Gant, J.C., Thibault, O., Blalock, E.M., Yang, J., Bachstetter, A., Kotick, J., et al., 2009. Decreased number of interneurons and increased seizures in neuropilin 2 deficient mice: implications for autism and epilepsy. Epilepsia 50, 629–645.
Harkin, L.A., McMahon, J.M., Iona, X., Dibbens, L., Pelekanos, J.T., Zuberi, S.M., et al., 2007. The spectrum of SCN1A-related infantile epileptic encephalopathies. Brain 130, 843–852.
Jhuang, H., Garrote, E., Yu, X., Khilnani, V., Poggio, T., Steele, A.D., et al., 2010. Automated home-cage behavioural phenotyping of mice. Nat. Commun. 1 http://dx.doi.org/10.1038/ncomms.1064.
Kalume, F., Yu, F.H., Westenbroek, R.E., Scheuer, T., Catterall, W.A., 2007. Reduced sodium current in Purkinje neurons from $Na_v1.1$ mutant mice: implications for ataxia in severe myoclonic epilepsy in infancy. J. Neurosci. 27, 11065–11074.
Kalynchuk, L.E., Pinel, J.P., Treit, D., Kippin, T.E., 1997. Changes in emotional behavior produced by long-term amygdala kindling in rats. Biol. Psychiatry 41, 438–451.
Kanki, H., Suzuki, H., Itohara, S., 2006. High-efficiency CAG-FLPe deleter mice in C57BL/6J background. Exp. Anim. 55, 137–141.
Kawaguchi, Y., Kondo, S., 2002. Parvalbumin, somatostatin and cholecystokinin as chemical markers for specific GABAergic interneuron types in the rat frontal cortex. J. Neurocytol. 31, 277–287.
Korotkova, T., Fuchs, E.C., Ponomarenko, A., von Engelhardt, J., Monyer, H., 2010. NMDA receptor ablation on parvalbumin-positive interneurons impairs hippocampal synchrony, spatial representations, and working memory. Neuron 68, 557–569.
McFarlane, H.G., Kusek, G.K., Yang, M., Phoenix, J.L., Bolivar, V.J., Crawley, J.N., 2008. Autism-like behavioral phenotypes in BTBR T+tf/J mice. Genes Brain Behav. 7, 152–163.
Moy, S.S., Nadler, J.J., Young, N.B., Perez, A., Holloway, L.P., Barbaro, R.P., et al., 2007. Mouse behavioral tasks relevant to autism: phenotypes of 10 inbred strains. Behav. Brain Res. 176, 4–20.
Murray, A.J., Sauer, J.F., Riedel, G., McClure, C., Ansel, L., Cheyne, L., et al., 2011. Parvalbumin-positive CA1 interneurons are required for spatial working but not for reference memory. Nat. Neurosci. 14, 297–299.
Nakatani, J., Tamada, K., Hatanaka, F., Ise, S., Ohta, H., Inoue, K., et al., 2009. Abnormal behavior in a chromosome-engineered mouse model for human 15q11–13 duplication seen in autism. Cell 137, 1235–1246.
Nakayama, T., Ogiwara, I., Ito, K., Kaneda, M., Mazaki, E., Osaka, H., et al., 2010. Deletions of SCN1A 5′ genomic region with promoter activity in Dravet syndrome. Hum. Mutat. 31, 820–829.
Nolan, K.J., Camfield, C.S., Camfield, P.R., 2006. Coping with Dravet syndrome: parental experiences with a catastrophic epilepsy. Dev. Med. Child Neurol. 48, 761–765.
Ogiwara, I., Miyamoto, H., Morita, N., Atapour, N., Mazaki, E., Inoue, I., et al., 2007. Na(v) 1.1 localizes to axons of parvalbumin-positive inhibitory interneurons: a circuit basis for epileptic seizures in mice carrying an Scn1a gene mutation. J. Neurosci. 27, 5903–5914.
O'Roak, B.J., Deriziotis, P., Lee, C., Vives, L., Schwartz, J.J., Girirajan, S., et al., 2011. Exome sequencing in sporadic autism spectrum disorders identifies severe de novo mutations. Nat. Genet. 43, 585–589.
Osaka, H., Ogiwara, I., Mazaki, E., Okamura, N., Yamashita, S., Iai, M., et al., 2007. Patients with a sodium channel alpha 1 gene mutation show wide phenotypic variation. Epilepsy Res. 75, 46–51.
Pompl, P.N., Mullan, M.J., Bjugstad, K., Arendash, G.W., 1999. Adaptation of the circular platform spatial memory task for mice: use in detecting cognitive impairment in the APP(SW) transgenic mouse model for Alzheimer's disease. J. Neurosci. Methods 87, 87–95.
Ragona, F., Brazzo, D., De Giorgi, I., Morbi, M., Freri, E., Teutonico, F., et al., 2010. Dravet syndrome: early clinical manifestations and cognitive outcome in 37 Italian patients. Brain Dev. 32, 71–77.
Riva, D., Vago, C., Pantaleoni, C., Bulgheroni, S., Mantegazza, M., Franceschetti, S., 2009. Progressive neurocognitive decline in two children with Dravet syndrome, de novo SCN1A truncations and different epileptic phenotypes. Am. J. Med. Genet. A 149A, 2339–2345.
Sadakata, T., Washida, M., Iwayama, Y., Shoji, S., Sato, Y., Ohkura, T., et al., 2007. Autistic-like phenotypes in Cadps2-knockout mice and aberrant CADPS2 splicing in autistic patients. J. Clin. Invest. 117, 931–943.
Selby, L., Zhang, C., Sun, Q.Q., 2007. Major defects in neocortical GABAergic inhibitory circuits in mice lacking the fragile X mental retardation protein. Neurosci. Lett. 412, 227–232.
Silverman, J.L., Yang, M., Lord, C., Crawley, J.N., 2010. Behavioural phenotyping assays for mouse models of autism. Nat. Rev. Neurosci. 11, 490–502.
Sontag, T.A., Tucha, O., Walitza, S., Lange, K.W., 2010. Animal models of attention deficit/hyperactivity disorder (ADHD): a critical review. Atten. Defic. Hyperact. Disord. 2, 1–20.
Steele, A.D., Jackson, W.S., King, O.D., Lindquist, S., 2007. The power of automated high-resolution behavior analysis revealed by its application to mouse models of Huntington's and prion diseases. Proc. Natl. Acad. Sci. U. S. A. 104, 1983–1988.
Sugawara, T., Mazaki-Miyazaki, E., Ito, M., Nagafuji, H., Fukuma, G., Mitsudome, A., et al., 2001. $Na_v1.1$ mutations cause febrile seizures associated with afebrile partial seizures. Neurology 57, 703–705.
Sugawara, T., Mazaki-Miyazaki, E., Fukushima, K., Shimomura, J., Fujiwara, T., Hamano, S., Inoue, Y., et al., 2002. Frequent mutations of SCN1A in severe myoclonic epilepsy in infancy. Neurology 58, 1122–1124.
Trantham-Davidson, H., Vazdarjanova, A., Dai, R., Terry, A., Bergson, C., 2008. Up-regulation of calcyon results in locomotor hyperactivity and reduced anxiety in mice. Behav. Brain Res. 189, 244–249.
Weiss, L.A., Escayg, A., Kearney, J.A., Trudeau, M., MacDonald, B.T., Mori, M., et al., 2003. Sodium channels SCN1A, SCN2A and SCN3A in familial autism. Mol. Psychiatry 8, 186–194.
Wolff, M., Cassé-Perrot, C., Dravet, C., 2006. Severe myoclonic epilepsy of infants (Dravet syndrome): natural history and neuropsychological findings. Epilepsia 47 (Suppl. 2), 45–48.
Yang, M., Crawley, J.N., 2009. Simple behavioral assessment of mouse olfaction. Curr. Protoc. Neurosci. 8 (Unit 8.24).
Yu, F.H., Mantegazza, M., Westenbroek, R.E., Robbins, C.A., Kalume, F., Burton, K.A., et al., 2006. Reduced sodium current in GABAergic interneurons in a mouse model of severe myoclonic epilepsy in infancy. Nat. Neurosci. 9, 1142–1149.

Cellular/Molecular

Rines E3 Ubiquitin Ligase Regulates MAO-A Levels and Emotional Responses

Miyuki Kabayama,[1] Kazuto Sakoori,[1] Kazuyuki Yamada,[3] Veravej G. Ornthanalai,[2] Maya Ota,[1] Naoko Morimura,[1] Kei-ichi Katayama,[1] Niall P. Murphy,[2] and Jun Aruga[1]

[1]Laboratory for Behavioral and Developmental Disorders, [2]Molecular Neuropathology Group, and [3]Support Unit for Animal Resources Development, RIKEN Brain Science Institute, Wako-shi, Saitama 351-0198, Japan

Monoamine oxidase A (MAO-A), the catabolic enzyme of norepinephrine and serotonin, plays a critical role in emotional and social behavior. However, the control and impact of endogenous MAO-A levels in the brain remains unknown. Here we show that the RING finger-type E3 ubiquitin ligase Rines/RNF180 regulates brain MAO-A subset, monoamine levels, and emotional behavior. Rines interacted with MAO-A and promoted its ubiquitination and degradation. Rines knock-out mice displayed impaired stress responses, enhanced anxiety, and affiliative behavior. Norepinephrine and serotonin levels were altered in the locus ceruleus, prefrontal cortex, and amygdala in either stressed or resting conditions, and MAO-A enzymatic activity was enhanced in the locus ceruleus in Rines knock-out mice. Treatment of Rines knock-out mice with MAO inhibitors showed genotype-specific effects on some of the abnormal affective behaviors. These results indicated that the control of emotional behavior by Rines is partly due to the regulation of MAO-A levels. These findings verify that Rines is a critical regulator of the monoaminergic system and emotional behavior and identify a promising candidate drug target for treating diseases associated with emotion.

Introduction

Mood and emotion are modulated by the brain monoamine transmitters norepinephrine (NE) and serotonin (5-HT), along with their essential catabolic enzyme monoamine oxidase A (MAO-A) (Shih et al., 1999). MAO-A has long been considered to be a central factor at the interface of psychiatry and pharmacology (Shih et al., 1999; Bortolato et al., 2008). MAO inhibitors and selective 5-HT or NE reuptake inhibitors are common pharmacotherapies for treating depression and anxiety disorders that work by increasing the levels of 5-HT and NE in the brain (Millan, 2003; Ravindran and Stein, 2010; Koen and Stein, 2011).

Consistent with the therapeutic importance of MAO-A, genetic evidence indicates that its expression levels in the brain may be a critical parameter for emotional and social behavior across species. Low-expression variants of MAO-A have been linked with increased risk of violent and aggressive behaviors (Hunter, 2010). A complete and selective deficiency of MAO-A was discovered in an extended family with a rare X-linked genetic mutation; members of this family showed Brunner syndrome, a collection of symptoms including impulsive aggression and antisocial behaviors (Brunner et al., 1993). In mice, male MAO-A knock-out (KO) mice exhibited enhanced aggression (Cases et al., 1995; Scott et al., 2008) and hypomorphic mutant mice were defective in social interactions (Cases et al., 1995; Scott et al., 2008; Bortolato et al., 2011). In contrast, promoter polymorphisms linked to high MAO-A activity are frequently observed in anxiety disorders and major depression in females (Deckert et al., 1999; Schulze et al., 2000; Samochowiec et al., 2004; Yu et al., 2005). In addition, MAO-A protein levels have been correlated with human emotional traits: a 34% increase in the brains of nonsmoking major-depression patients (Meyer et al., 2006) and an inverse correlation with the severity of antisocial traits (Alia-Klein et al., 2008). This evidence suggests that MAO-A levels need to be finely tuned for appropriate emotional responses.

We hypothesized that the ubiquitin proteasomal system (UPS) may have a vital role in MAO-A metabolism because UPS controls protein homeostasis for neuronal properties such as synaptic plasticity (Hershko and Ciechanover, 1998; Pickart, 2001; Johnston and Madura, 2004; Moriyoshi et al., 2004; Yao et al., 2007) and memory formation (Gong et al., 2006; Lee et al., 2008; Sakurai et al., 2008). E3 ubiquitin ligases play a key role in UPS function by determining the specificity and timing of ubiquitination and subsequent degradation of its substrates (Pickart, 2001). However, whether E3 ligases play a role in controlling emotional and social responses by modulating the monoamine levels is virtually unknown. In particular, the protein degradation mechanism that targets monoamine-metabolizing enzymes, including MAO, in the brain is largely unknown, although MAO proteins are ubiquitinated in cell culture (Jiang et al., 2006), suggesting that the mechanism is mediated by UPS.

Received Dec. 14, 2012; revised June 15, 2013; accepted June 21, 2013.

Author contributions: M.K., K.S., and J.A. designed research; M.K., K.S., K.Y., V.G.O., M.O., N.M., K.K., N.P.M., and J.A. performed research; M.K., K.S., K.Y., V.G.O., M.O., N.M., K.K., N.P.M., and J.A. analyzed data; M.K. and J.A. wrote the paper.

This study was supported by RIKEN Brain Science Institute funds and by a Ministry of Education, Culture, Sports, Science, and Technology, Japan Grant-in-Aid for Scientific Research A (Grant #21240031). We thank Drs. Charles Yokoyama and Alexandra V. Terashima for helpful comments on the manuscript, Dr. Hiroshi Kawabe for technical advice and valuable discussion, and members of RIKEN Brain Science Institute Research Resources Center for assistance in animal maintenance and RT-PCR analysis.

The authors declare no competing financial interests.

Correspondence should be addressed to Jun Aruga, Laboratory for Behavioral and Developmental Disorders, RIKEN BSI, 2–1 Hirosawa, Wako-shi, Saitama 351-0198, Japan. E-mail: jaruga@brain.riken.jp.

DOI:10.1523/JNEUROSCI.5717-12.2013

 0270-6474/13/3312940-14$15.00/0

Here we report the role of an E3 ligase, Rines, in monoamine control and in emotional and social behaviors. Analysis of Rines KO mice demonstrates that Rines controls MAO-A protein and monoamine levels as well as emotional and social behaviors.

Materials and Methods

Animals. All animal experiments were performed according to the guidelines for animal experimentation at RIKEN. The mice were housed on a 12 h:12 h light/dark cycle, with the dark cycle occurring from 20:00 to 8:00. All mice used were littermates from mated heterozygotes. All behavioral tests in this study were performed with adult male mice.

Generation of Rines mutant mice. Rines mutant mice were generated as described previously (Katayama et al., 2010). To construct the Rines-targeting vector, overlapping Rines genomic clones were isolated from a phage library derived from mice of the 129 SV strain (Stratagene). The targeting construct contained the 7.6 and 3 kb homology regions and the 11 kb fragment containing the exon 6 of Rines was replaced with the phosphoglycerol kinase (PGK) neoexpression cassette flanked by a loxP sequence. E14 embryonic stem cells were electroporated with the targeting construct and selected with G418. Drug-resistant clones were analyzed by Southern blotting. BglII-digested genomic DNA was hybridized with a 0.9 kb 3′ genomic fragment, which corresponded to the genomic sequence outside of the targeting vector and a 0.6 kb PstI PGK neoprobe, respectively. Chimeric mice were generated by the injection of targeted embryonic stem cells into C57BL/6J blastocysts. To excise the PGK neocassette, mice with germline transmission were first mated with transgenic mice expressing Cre recombinase under the control of the cytomegalovirus immediate early enhancer chicken β-actin hybrid promoter. Correct excision of the PGK neocassette was confirmed by Southern blot. Mice carrying the mutated Rines allele were backcrossed to C57BL/6J for more than six generations before analysis. Genotyping of progenies was performed by Southern blot or RT-PCR analysis of DNA isolated from brain samples. In all experiments using Rines mutant mice, the controls were sex-matched littermate wild-type (WT) mice.

Antibodies. A rabbit polyclonal antibody to Rines was raised against a GST fusion protein of mouse Rines (residues 1–150). An obtained antibody in antisera was purified by affinity chromatography with the GST-Rines (residues 1–150). The following antibodies were obtained from commercial sources: MAO-A (T-19; Santa Cruz Biotechnology) for immunostaining; MAO-A IP-WB antibody pair (H00004128-PW1) for immunoprecipitation and immunoblotting; tyrosine hydroxylase (TH; Millipore); ubiquitin-protein conjugate (Enzo Life Sciences); β-actin (Sigma); HA (Sigma or 12CA5; Roche); Flag (M2; Sigma); and Myc (9E10; Santa Cruz Biotechnology).

RNA extraction and RT-PCR. RNA extraction and RT-PCR were performed as described previously (Inoue et al., 2004). RNAs were isolated from mice brains with TRIzol reagent (Invitrogen). After DNaseI treatment, reverse transcription was performed with M-MLV reverse transcriptase (Invitrogen) or Superscript II reverse transcriptase (Invitrogen). G3PDH was evaluated to monitor RNA recovery. The PCR cycles, annealing temperature, and primer sequences were as follows: 22 cycles, 68°C, mouse (m) G3PDH F: 5′-TGTTCCTACCCCCAATGTGT-3′; mG3PDH reverse: 5′-TGTGAGGGAGATGCTCAGTG-3′; 30 cycles, 58°C, mRines 1 forward: 5′-ATGAAAAGAAGCGAAGAGTCGACAAGTA-3′, mRines 1 reverse: 5′-CGCGAATTCTCCTGAGTATTTACCCTGC-3′, mRines 2 forward: 5′-CGCGGATCCCTGATGGATCTGCCCTCAG-3′, mRines 2 reverse: 5′-CGCGAATTCCATGTAGCTGTCCTTCTCC-3′, mRines 3 forward: 5′-CGCGGATCCGCGACGTATTTTGAGATGA-3′, mRines 3 reverse: 5′-CGCGAATTCGAATGGCAGGCTGTTAGCG-3′, mRines 4 forward: 5′-CGCGGATCCACTCTGCGAAGGCAGCAGA-3′, mRines 4 reverse: 5′-CTAAAACGGAAAGAAAAAAATAGCAAAG-3′.

To quantify Rines expression in whole brains (1- to 10-month-old WT mice) and brain punch regions (3-month-old WT mice), a quantitative real-time PCR system (ABI7900HT; Applied Biosystems) with TaqMan MGB (Applied Biosystems) was used. For quantification of Rines expression in brain punch regions, circular tissue punches were taken of the CA3 and dentate gyrus of the hippocampus, medial prefrontal cortex, basolateral and cortical nuclei of the amygdala, nucleus accumbens, corpus striatum, substantial nigra, raphe nuclei, and locus ceruleus (LC) using disposable biopsy needles (Biopsy Punch; Kai Medical) with diameters of 1, 1, 1, 2, 1.5, 1.5, 1.5, 1.5, and 2 mm, respectively, from 150-μm-thick frozen coronal brain sections of 3-month-old male C57BL/6J mice. PCR was started at 95°C for 10 min, followed by 50 cycles at 95°C for 15 s and 60°C for 60 s. The intensity relative to GAPDH (4352339E; Applied Biosystems) was calculated and the relative amount of mRNA was plotted. The TaqMan Rines MGB probe was 5′-AGTGGACAGTTGGGAAA-3′ and the Rines primer sequences were: forward: 5′-TCAGCTGCTTGCTGCAGAAG-3′ and reverse: 5′-CCCCACAGAAAGGACAATTCA-3′. Real-time RT-PCR was used for quantification of MAO-A, MAO-B, DBH, NET, VMAT2, COMT, and Rines expression in the LC of WT and Rines KO mice using a Rotor-Gene Real-time PCR system (QIAGEN) with SYBR Green Real-time PCR Master Mix (Applied Biosystems). Circular tissue punches (1.5 mm in diameter) of the LC region were taken from 150-μm-thick frozen coronal brain sections of 9-month-old mice ($n = 7$ per group). PCR was started at 95°C for 15 min, followed by 40 cycles at 95°C for 10 s, 55°C for 20 s, and 72°C for 20 s. The amplification specificity was tested by a dissociation curve (72–95°C). The intensity relative to G3PDH was calculated. The primer sequences were as follows: mRines forward: 5′-TTCCTGCGCTCTGCCAGCTTC-3′, mRines reverse: 5′-TGTAGCCATCGTTCGCGCCT-3′, mMAO-A forward: 5′-AACGACTTGCTAAACTACAT-3′, mMAO-A reverse: 5′-AGCAGAGAAGAGCCACAGAA-3′, mMAO-B forward: 5′-GAAAACTGGTACGTCTCACC-3′, mMAO-B reverse: 5′-GAGCTGTTGCTGACAAGATG-3′, mNET forward: 5′-TGGTTTTATGGTGTGGACAG-3′, mNET reverse: 5′-GGTGCTCATTCTCCGGGGTG-3′, mDBH forward: 5′-TGACGGGCAGGAAGGTGGTTAC-3′, mDBH reverse: 5′-CTGGAAGTGGGGGCTGTAGTGG-3′, mCOMT forward: 5′-TGGCACAAAGGAGCAGCGCATC-3′, mCOMT reverse: 5′-ACCCACGTTCATGGCCCACTC-3′, mVMAT2 forward: 5′-AGCGCTCACAGCCTCCACTTC-3′, mVMAT2 reverse: 5′-CGTGGCATTCCCCGTGAACAC-3′, mG3PDH forward: 5′-TCCACCACCCTGTTGCTGTA-3′, and mG3PDH reverse: 5′-ACCACAGTCCATGCCATCAC-3′.

Subcellular fractionation. The mouse brain tissues were isolated and homogenized in a homogenization buffer (5 mM Tris-HCl, pH 8.0, 0.32 M sucrose, 1 mM EDTA, 1 mM 2-mercaptoethanol, and complete protease inhibitor mixture; Roche). This homogenate was centrifuged at 1800 × *g* for 10 min and the supernatant was further centrifuged at 10,000 × *g* for 15 min. Subsequently, the supernatant was centrifuged at 75,000 × *g* for 60 min, after which time the pellet (microsome fraction) was resuspended in SDS lysis buffer (50 mM Tris-HCl, pH 7.5, 0.5 mM EDTA, 1% SDS, and 1 mM dithiothreitol) and diluted 5-fold by adding 0.5% NP-40.

Behavioral tests. The mice were kept in isolation for at least 1 week before the behavioral experiments. The laboratory was air-conditioned, with the temperature and humidity maintained within ~22–23°C and 50–55%, respectively. The experiments were conducted during the light phase (11:00–17:30), except for the home cage activity and resident-intruder tests. Male mice 4.5–8 months old (open field, elevated plus maze, light–dark box, passive avoidance, forced swimming, resident-intruder, hidden cookie, hot plate, and tail-flick tests), 12 months old (social interaction test), or 2–3 months old (other behavioral tests) were used.

Open field test. The open-field test was performed as described previously (Sakatani et al., 2009). Each mouse was placed in the center of an open-field apparatus (50 × 50 × 40 [H] cm) illuminated by light-emitting diodes (70 lux at the center of the field) and its horizontal movements were monitored for 15 min with a CCD camera. Distance traveled (cm) and duration (s) in the center area of the field (36% of the field) were adopted as the indices. The relevant data were collected every minute and analyzed with ImageJ OF4 software (O'Hara).

Elevated plus-maze test. The elevated plus-maze test was conducted as described previously (Satoh et al., 2007). Mice were tested for anxiety-like behavior on a standard plus-maze apparatus (closed arms, 25 × 5 × 15 [H] cm; open arms, 25 × 5 × 0.3 [H] cm arranged orthogonally) 60 cm above the floor. Illuminance was 70 lux at the center platform of the maze (5 × 5 cm). Each mouse was placed on the center platform facing an open arm and then was allowed to move freely in the maze for 5 min. Total distance traveled, percentage of time in the open arms, and per-

centage of open arm entries were measured as indices. Data were collected and analyzed using ImageJ EPM software (O'Hara).

Light–dark box transition test. The light–dark box transition test was performed as described previously (Yamada et al., 2003). The apparatus consisted of a cage (40 × 20 × 20 cm) equally divided in two by a black partition containing a small opening. One chamber was open and brightly illuminated (250 lux), whereas the other was closed and dark. Mice were placed into the light side and allowed to move freely between the two chambers for 10 min. Three parameters were measured with ImageJ LD software (O'Hara): latency to enter the light compartment, number of entries into the light compartment, and duration in the light compartment.

Passive avoidance test. The passive avoidance test was performed as described previously with slight modification (Yamada et al., 2003). A single mouse was introduced into a light compartment of a light–dark box (Muromachi-kikai). During habituation, 1 min after introduction, the sliding door between the light and dark compartments was opened and the mouse was allowed to freely explore the box for 4 min with the sliding door open and then returned to its home cage. For conditioning, which was performed 24 h after habituation, the mouse was introduced into the light compartment; 1 min after introduction, the sliding door was opened and when both hindlimbs of the mouse had entered the dark box, an electrical foot shock was delivered via the floor grid in the dark compartment (0.2 mA for 3 s using a shock generator–scrambler; Muromachi-kikai). When the mouse had entered the light box, the sliding door was closed; the mouse was left in the light box for 2 min and then returned to its home cage. Testing was performed 24 h after conditioning by reintroducing the mouse into the light compartment of the light–dark box. The latency for the mouse to enter the dark compartment was measured (light–dark latency, with a 999 s cutoff).

Forced swimming test. The forced swimming test was performed as described previously with slight modification (Porsolt et al., 1978; Porsolt et al., 1979; Duncan et al., 1993). Each mouse was placed for 15 min in a glass cylinder (30 cm high, 10 cm in diameter) containing 10 cm of water maintained at 24–25°C. After 24 h, each mouse was replaced for 5 min in the glass cylinder with water. The time spent immobile on days 1 and 2 was recorded visually during the test period. In the forced swim test, immobility is induced in the test swim by previous exposure to the conditioning swim (Duncan et al., 1993).

Hot plate and tail flick tests. In the hot plate test, the surface of the hot plate (Ugo Basile) was heated to a constant temperature of 52 ± 0.5°C. Each mouse was placed on the hot plate, which was surrounded by a clear acrylic cage (18 cm high, 19 cm in diameter, open top). The latencies to respond with licking of the forepaws and flinching of the hindpaws were measured visually. The cutoff time was 60 s. In the tail flick test, each mouse was individually restrained on the radiant heat meter (Ugo Basile) and focused heat was applied to the surface of the tail at a distance 2–3 cm from its tip. The latency to reflexive removal of the tail from the heat was recorded manually as the tail flick latency.

Social interaction test (encounter method). The social interaction test was performed as described previously (Kato et al., 2008). A subject mouse was individually placed at the center of a white-colored open field (40 × 40 × 30 [H] cm). Immediately thereafter, a target mouse was also introduced into the same open field. The duration of contact behavior was then measured for 6 h. Contact or separation was expressed as "1" or "2," respectively. That is, the software returned a value of "1" when the mice were in contact and a value of "2" when they were separated. Data were collected and analyzed using a personal computer and commercially available software (Time HC; O'Hara).

Resident-intruder test. The resident-intruder test was performed during the dark phase (21:00–23:00). The times spent in following, approaching, and sniffing the intruder mice (12-week-old male BALB/c mice housed in groups) were measured for 5 min. The latency to the first attack, duration of fighting, and number of bouts of fighting were measured for 10 min. Social behaviors were measured with video recordings by well trained observers who were blind to the genotypes.

Home cage activity. The spontaneous activity of mice in their home cage was measured using a 24-channel ABsystem 4.0 (Neuroscience). Cages were individually set into compartments made of stainless steel in the negative breeding rack (JCL). An infrared sensor mounted on the ceiling of each compartment detected the movements of the mice. Home cage activity was measured for 1 week from the afternoon of the day of transfer to the behavioral laboratory (day 1) until the same day of the next week (day 8).

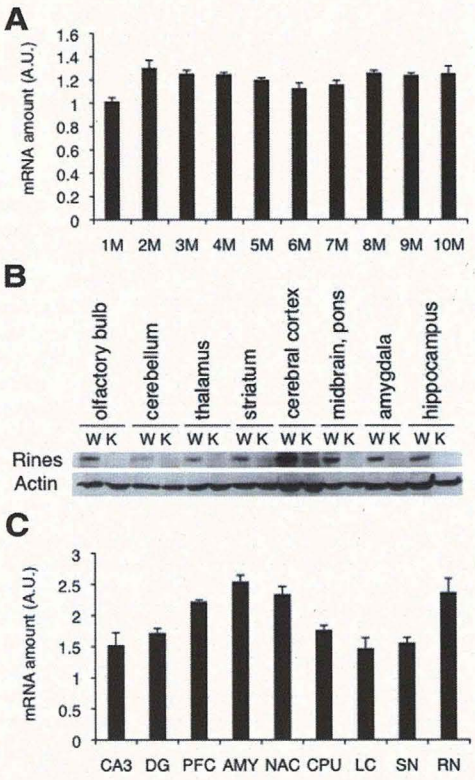

Figure 1. Rines expression in the mouse brain. ***A***, ***C***, Quantitative RT-PCR analysis. ***A***, Developmental changes in the Rines mRNA level in the brain from 1 to 10 months of age (M). ***B***, Distribution of the Rines protein in adult brain. Microsomal fractions from WT (W) and Rines KO (K) were subjected to immunoblotting analysis using anti-Rines and anti-β-actin antibodies. ***C***, Regional expression of Rines in adult (12 weeks) brain. CA3 and DG, dentate gyrus of hippocampus; PFC, prefrontal cortex; AMY, amygdala; NAC, nucleus accumbens; CPU, corpus striatum; LC, locus ceruleus; SN, substantia nigra; RN, raphe nuclei; AU, arbitrary unit.

Hidden cookie test. The hidden cookie test was performed as described previously with slight modification (Irie et al., 2012). Mice first were habituated overnight to butter cookies in the home cage. The next day, the mice were food deprived for 24 h. The test was conducted in a new cage. A piece of butter cookie (0.75 mg) was placed at a randomly chosen area on the cage floor and then the entire cage floor was covered with corncob bedding to a depth of 4 cm. The subject was placed into the cage and latency to find and eat the cookie was recorded.

Auditory startle response and prepulse inhibition tests. Each mouse was placed into a small cage for measuring the auditory startle response (30 or 35 mm in diameter, 12 cm long), after which the cage was set on a sensor block installed in a sound-proof chamber (60 × 50 × 67 [H] cm). A dim light was mounted on the ceiling of the sound-proof chamber (10 lux at the center of the sensor block) and a 65 dB white noise was presented as background noise. In the auditory startle response test, mice were acclimated to the experimental condition for 5 min, after which time the experimental session began. In the first session, 10 startle stimuli (120 dB, 40 ms) were presented at random intertrial intervals (10–20 s). In the second session, the startle responses to stimuli of various intensities were assessed. White noise stimuli ranging in intensity from 70 to 120 dB (70, 75, 80, 85, 90, 95, 100, 110, and 120 dB; 40 ms) were presented 5 times each in quasirandom order at random intertrial intervals (10–20 s). In the prepulse inhibition session, the mice experienced five types of trials: no stimulus; startle stimulus (120 dB, 40 ms) alone; 70 dB prepulse (20

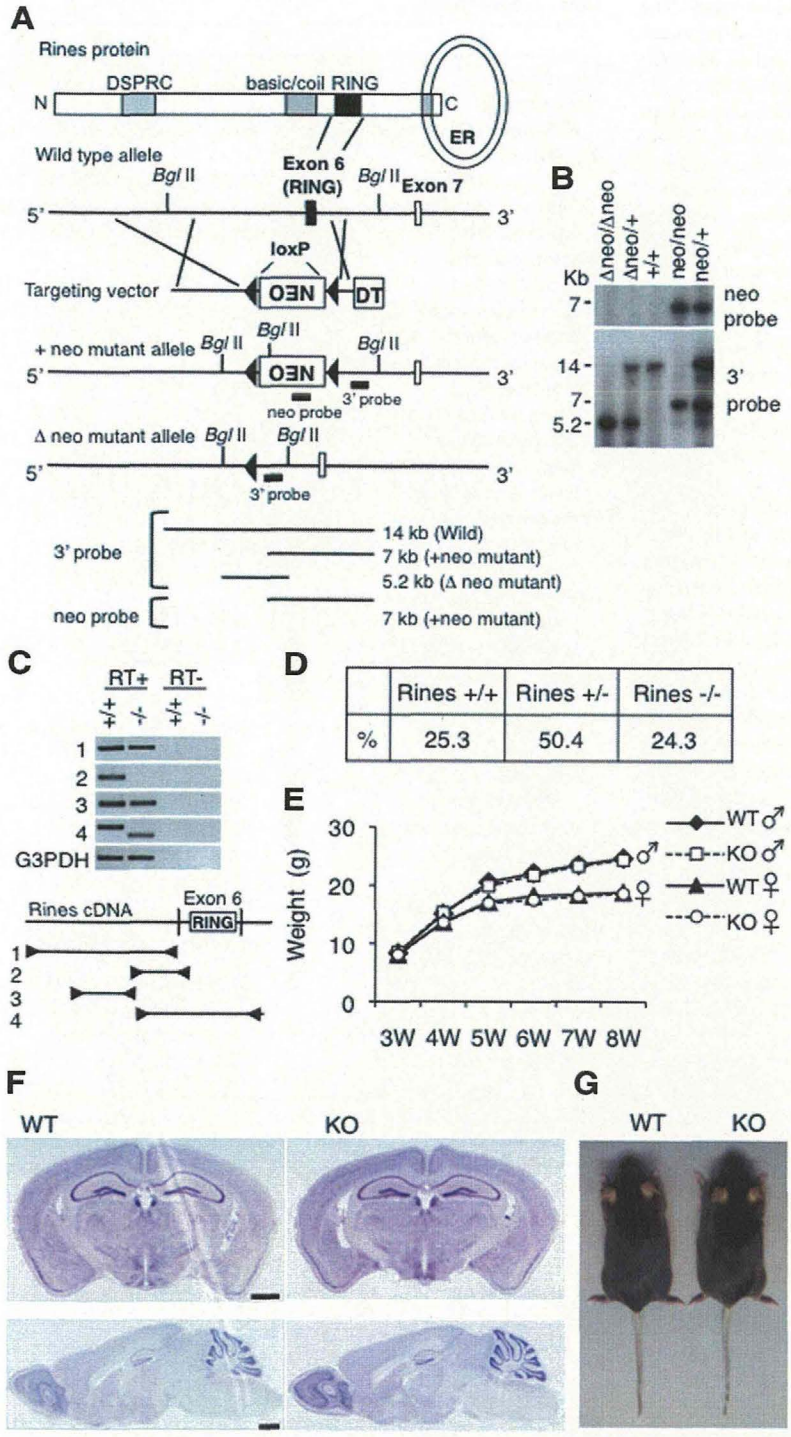

Figure 2. Rines KO strategy and histology of Rines KO brain. ***A***, Structures of the Rines protein, gene, targeting vector, and mutated allele. The sixth exon, which contains the RING finger domain (black box), was replaced with the neomycin resistance gene cassette (NEO), excised by Cre recombinase in germline cells and flanked by loxP sequences. The location of the 3′ and neoprobes used for Southern blotting and the expected size of the hybridizing fragments with 3′ and neoprobes after BglII digestion are shown. ***B***, ***C***, Confirmation of the mutant alleles by Southern blotting (***B***) and RT-PCR analysis (***C***). The locations of the 1-4 primers used for the RT-PCR analysis are shown. ***D–F***, Survival rates, body growth, and brain histology of Rines KO mice. ***D***, Genotype percentages in the 2162 3-week-old progenies from interheterozygote mating. There were no significant differences in the percentages of each genotype when we analyzed the data by a χ^2 test ($p = 0.74$). ***E***, Body weight curves of male and female WT and Rines KO mice from weaning period (3 weeks) to 8 weeks. Male: WT, $n = 19$; KO, $n = 21$, Female: WT, $n = 18$; KO, $n = 21$. ***F***, Cresyl violet staining of brain sections of 2-month-old WT and Rines KO mice. Scale bar, 1 mm. ***G***, Dorsal views of WT and Rines KO mice at 7.5 months.

ms, lead time 100 ms) and 120 dB pulse; 75 dB prepulse (20 ms, lead time 100 ms) and 120 dB pulse; and 80 dB prepulse (20 ms, lead time 100 ms) and 120 dB pulse. Each trial type was repeated 10 times in quasirandom order at random intertrial intervals (10–20 s). In the final session, 10 startle stimuli (120 dB, 40 ms) were again presented at random intertrial intervals (10–20 s). Commercially available apparatuses and data analysis software were used (Mouse Startle software; O'Hara).

Morris water maze test. A circular maze made of white plastic (1 m in diameter, 30 cm in depth) was filled with water to a depth of ~20 cm (22–23°C). The water was colored with white paint so that the mice could not see the platform (20 cm high, 10 cm in diameter; 1 cm below the surface of water) or other cues under the water. Various extramaze landmark cues (i,e., a calendar, figure, and plastic box) were visible to the mice in the maze. Movements in the maze were recorded and analyzed with ImageJ WM software (O'Hara). Each mouse received six trials (one session) daily for four consecutive days. Each acquisition trial began when an individual mouse was placed into the water facing the outer edge of the maze at one of four designated starting points quasirandomly. The submerged platform remained constant for each mouse throughout testing. A trial ended when the mouse reached the platform, and the latency and distance swum were measured. Mice that did not reach the platform within the cutoff time of 60 s were removed from the water and placed on the platform for 30 s before being toweled off and placed back into their home cage. The intertrial interval was ~6 min. In the probe test conducted after the 4 d of training, the platform was taken away and each mouse was placed into the water at the position opposite to the target platform and allowed to swim for 60 s. The distance swum, number of crossings, positions of the target and three nontarget platforms, and times spent in the quadrants of the four platforms were measured.

Rotarod test. The time that a mouse placed on a rotating rod (O'Hara) could maintain its balance walking on the rod was measured. The speed of rotation, which was 4 rpm on day 1, was increased from 4 to 40 rpm over a 4 min period and then maintained at 40 rpm for 1 min on days 2–5. The mice were tested during a single 2 min trial on day 1 and during 4 trials, each with a maximum time of 300 s (intertrial interval, 20–30 s) on days 2–5. The time between placement and falling off or revolving around the rod was manually recorded.

Drug administration tests. The average volume of water consumed per day was measured before the administration of the nonselective and irreversible MAO inhibitor tranylcypromine (TCP; Sigma). TCP (~3 mg/kg) dissolved in drinking water was provided *ad libitum* chronically for 11–23 d. Subsequently, the open field, light–dark box, and forced swimming tests were performed as described above except that the mice were kept in groups of 3–5 before the tests. Tests were performed with male mice, 6–7 months old (open

field) or 6–17 months old (light–dark box and forced swimming tests). The immobility time in the forced swimming test was analyzed using the Supermex apparatus and CompACT FSS software (Muromachi-kikai). The TCP dose was chosen to fully inhibit MAO-A (Maki et al., 2000; Weber et al., 2009). Clorgyline (Sigma) was dissolved in sterile saline. The mice were kept in isolation for at least 1 week before the behavioral experiments and testing was conducted on 6- to 7-month-old male mice. On the conditioning day of the passive avoidance test, the mice were injected intraperitoneally with 5 ml/kg sterile saline or clorgyline (0.1–1 mg/kg) 2.5 h before the electric foot shock. This interval was chosen because 2–4.5 h after clorgyline pretreatment (0.1–10 mg/kg) in mice, apparent monoamine turnover in the brain attenuated without changes in horizontal locomotor activities (Kitanaka et al., 2006).

Neurochemical analysis. Quiet (control) male mice, 7–8 months old, were left undisturbed in their home cages. Mice of comparable age in the foot shock group were delivered 20 shocks (0.2 mA, 1 s) randomly during a 20 min period in a plastic chamber equipped with a stainless steel grid floor wired to a shock generator. This stressful treatment alters monoamine turnover and behavioral responses (Swiergiel et al., 2008). The mice were decapitated immediately after the foot shock period. The brains were collected, and 150-μm-thick frozen coronal sections were prepared. Circular tissue punches were collected from the medial prefrontal cortex, basolateral and cortical nuclei of the amygdala, substantia nigra, raphe nuclei, and LC using disposable biopsy needles (Biopsy Punch; Kai Medical) with diameters of 1, 2, 1.5, 1.5, and 2 mm, respectively. The samples were homogenized in 0.1 M perchloric acid containing 0.1 mM EDTA and centrifuged for 15 min at 20,000 $\times$ *g* at 4°C. The supernatant was then filtered through 0.22 μm polyvinylidene fluoride (PVDF) micropore filters (Millipore), and the filtrate was analyzed by high-pressure liquid chromatography (HPLC) coupled to an electrochemical detection system (graphite electrode vs Ag/AgCL reference, Eicom). Briefly, a Prepak AC-ODS 4.0 $\times$ 5.0 mm precolumn and an Eicompak SC-5ODS 3.0 $\times$ 150 mm column were used for separations; the perfusate was a mobile phase consisting of 44.7 mM citrate, 40.3 mM sodium acetate, 15% methanol, 190 mg/L sodium 1-octanesulfonate, and 5 mg/L EDTA, adjusted to pH 3.7 using glacial acetic acid and pumped at a rate of 0.5 ml/min. The working electrode (WE-3G) potential was set at +0.5 V. The column temperature was maintained at 25°C. The HPLC data were collected automatically and analyzed by EZChrom Elite (Scientific Software). Protein was measured using a DC Protein Assay kit (Bio-Rad). All analyte information, including the retention times, peak heights, concentrations, and recovery rate of the internal standards, were calculated in relation to standard curves generated for known concentrations of external standards run daily.

Measurement of MAO-A activity. Circular tissue punches of the medial prefrontal cortex, basolateral nucleus of the amygdala, substantia nigra, raphe nuclei, and LC were collected using disposable biopsy needles (Biopsy Punch; Kai Medical) with diameters of 1, 1, 1.5, 1.5, and 1.5 mm, respectively, from 150-μm-thick frozen coronal brain sections of 7- to 9-month-old male mice. MAO-A activity was measured with an MAO-Glo Assay kit (Promega). Tissues were homogenized in ice-cold 100 mM HEPES-KOH, pH 7.4, 5% glycerol, and a complete protease inhibitor mixture (Roche) solution. An aliquot of the homogenate corresponding to 2 μg of protein was used for each MAO-A reaction. The luminescent signal was measured with a Mini Lumat LB9506 luminometer (Berthold Technology).

Immunofluorescence staining. Immunofluoresence staining was performed as described previously (Inoue et al., 2004). Male mice 7–8 months old were fixed in 4% paraformaldehyde. Cryosections of their brains (20 μm in thickness) were prepared and reacted with primary antibodies after blocking with 2% normal donkey serum (Jackson ImmunoResearch) and 0.1% Triton X-100 in PBS. Immunopositive signals were detected with Alexa Fluor 488- or Alexa Fluor 594-labeled secondary antibodies (Invitrogen). Fluorescence-labeled preparations were imaged under a Fluoview FV1000 confocal microscope (Olympus). Signal intensities were measured with MetaMorph software (Molecular Devices). The relative area of DAPI staining and the number of stained cells in the LC regions were measured with ImageJ software. The LC regions were defined by TH-immunostaining clusters. For morphometrical analyses, cryosections of brains were stained with cresyl violet, thionine, or toluidine blue.

cDNA cloning and plasmid construction. Full-length mouse MAO-A cDNA was obtained from a FANTOM3 clone set (Carninci et al., 2005). Flag- and HA-tagged MAO-A expression vectors were constructed by inserting the epitope tags and the protein coding region in-frame into the

Table 1. Behavioral tests

	WT	KO
Body weight (g)	30.2 ± 0.39	30.4 ± 0.50
Home cage activity		
Whole day (per 30 min on days 1–7) (AU)	231.31 ± 15.19	224.43 ± 16.32
Open field test		
Total distance (cm)	5625.78 ± 258.56	6084.73 ± 377.61
Total number of moving events	257.5 ± 5.08	231.0 ± 6.04**
Total center time (s)	214.41 ± 14.42	139.58 ± 8.83***
Elevated plus maze test		
Total distance (cm)	607.54 ± 38.66	609.79 ± 52.59
Spent time in open arms (%)	12.65 ± 3.04	1.78 ± 0.50*
Entries into open arms (%)	24.59 ± 4.32	13.77 ± 3.32
Light-dark box transition test		
Total distance (cm)	1079.91 ± 117.79	969.80 ± 119.51
Latency to enter dark box (s)	33.68 ± 8.36	28.44 ± 9.78
Light/dark transitions	26.16 ± 1.72	25.69 ± 2.00
Distance traveled in light box	35.09 ± 1.47	37.91 ± 1.69
Time in light box (%)	34.80 ± 2.09	36.53 ± 2.59
Passive avoidance test		
Latency in conditioning (s)	10.5 ± 2.05	11.1 ± 4.13
Latency in 24 h test (s)	553.5 ± 106.18	71.7 ± 31.47**
Forced swimming test		
Immobility time on day 1 (%)	38.16 ± 2.63	38.42 ± 2.90
Immobility time on day 2 (%)	51.87 ± 3.74	33.56 ± 3.70**
Morris water maze test		
Escape latency in training (s)		
Day 1	45.54 ± 3.42	44.94 ± 3.64
Day 4	20.50 ± 3.96	18.91 ± 2.52
Probe test		
Time in target (%)	35.92 ± 5.18	36.58 ± 3.71
Number of target crossings (%)	42.95 ± 11.61	38.84 ± 5.21
Tail flick test (latency) (s)	2.29 ± 0.09	2.42 ± 0.09
Hot plate test		
Licking of forepaws (latency)	18.56 ± 0.74	19.54 ± 1.44
Flinch of hindpaws (latency) (s)	26.46 ± 1.43	27.20 ± 1.76
Rotarod test (latency to fall) (s)		
Day 1	124.70 ± 11.07	108.95 ± 11.36
Day 4	163.53 ± 10.33	162.10 ± 14.07
Auditory startle response (AU)		
Intensity: 70 dB	0.10 ± 0.01	0.11 ± 0.01
Intensity: 120 dB	3.35 ± 0.49	2.63 ± 0.29
Prepulse inhibition test (startle stimulus:120 dB) (%inhibition)		
Intensity: 70 dB	14.88 ± 3.97	2.74 ± 6.38
Intensity: 80 dB	33.78 ± 5.23	37.53 ± 12.72
Social interaction test		
5 h	1.39 ± 0.094	1.16 ± 0.038*
6 h	1.43 ± 0.073	1.24 ± 0.042*
Resident-intruder test		
Social investigation duration (s)	55.34 ± 6.39	84.78 ± 10.04*
Latency to first attack (s)	450.96 ± 65.26	506.46 ± 62.37
Fighting duration (s)	3.41 ± 2.15	0.96 ± 0.77
Number of fighting bouts	1.3 ± 0.6	0.7 ± 0.6
Hidden cookie test (latency to find food) (s)	150.04 ± 15.80	159.24 ± 12.21

Data represent the mean ± SEM. *$p < 0.05$, **$p < 0.01$, ***$p < 0.001$, Student's *t* test (open field, passive avoidance, social interaction, and resident-intruder tests) or Mann–Whitney *U* test (elevated plus maze and forced swimming tests) compared with WT mice. For home cage activity, passive avoidance test, Morris water maze test, rotarod test, auditory response test, prepulse inhibition test, social interaction test, resident-intruder test, and hidden cookie test: WT, $n = 10$; KO, $n = 10$. For body weight: WT, $n = 59$; KO, $n = 50$. For open field test: WT, $n = 16$; KO, $n = 12$. For elevated plus maze test: WT, $n = 37$; KO, $n = 30$. For light–dark box transition test: WT, $n = 38$; KO, $n = 32$. For forced swimming test and tail flick test: WT, $n = 22$; KO, $n = 20$. For hot plate test: WT, $n = 21$; KO, $n = 20$. AU, arbitrary unit.